Sustainable Energy & Fuels

Experimental-Based Mechanistic Study and Optimization of Hydrothermal Liquefaction of Anaerobic Digestates

Journal:	*Sustainable Energy & Fuels*
Manuscript ID	SE-ART-02-2022-000206.R1
Article Type:	Paper
Date Submitted by the Author:	24-Mar-2022
Complete List of Authors:	Sudibyo, Hanifrahmawan; Cornell University School of Chemical and Biomolecular Engineering, Chemical and Biomolecular Engineering; Universitas Gadjah Mada Departemen Teknik Kimia, Teknik Kimia Pecchi, Matteo; Cornell University School of Chemical and Biomolecular Engineering, Chemical and Biomolecular Engineering Tester, Jefferson; Cornell, School of Chemical and Biomolecular Engineering

ARTICLE

Experimental-Based Mechanistic Study and Optimization of Hydrothermal Liquefaction of Anaerobic Digestates

Received 00th January 20xx,
Accepted 00th January 20xx

DOI: 10.1039/x0xx00000x

Hanifrahmawan Sudibyo[a,b,c,*], Matteo Pecchi[a,b], Jefferson William Tester[a,b]

Valorization of agricultural and food waste digestates is crucial for sustainable waste management to reduce environmental impacts and improve the economics of commercial farms. Hydrothermal liquefaction (HTL) of anaerobic digestates were evaluated to recover resources by converting them into carbon-dense biocrude oil and nutrient-rich HTL aqueous phase (HTL-AP) coproduct. The effects of HTL temperature (280–360°C), reaction time (10-50 min), feedstock pH (2.5–8.5), digestate salt content (1–5wt%), and digestate cellulose-to-lignin ratio (0.2–1.8) on energy and nutrient recovery were systematically investigated in a set of well-designed experiment following a half-fractional central composite protocol. Response surface analysis combined with HTL products characterization and comparative literature study produced a comprehensive reaction pathway for HTL of anaerobic digestate. Moreover, this analysis revealed the importance of acidic feedstocks (pH 3.00–5.53), high reaction temperatures (337–360°C), and reaction times <45 or 45–50 min for digestates with Cel/Lig >1 or <1, for maximizing the energy recovered in biocrude (high carbon yield and low heteroatom content) and the amounts of P, NH3-N, and Mg distributed in HTL-AP. Acidic conditions catalyzed biocrude production, inhibited Maillard reaction (lowering nitrogen content in biocrude), and partitioned nutrients into HTL-AP. Higher reaction temperatures coupled with longer reaction times activated hydro-denitrogenation and deoxygenation reactions to improve biocrude quality. This work provides not only validated methods to achieve targeted resource recovery for specific feedstock compositions using HTL, but also comprehensive mechanistic understanding of the HTL of biomass waste for controlling target product characteristics.

Keywords: anaerobic digestate; hydrothermal liquefaction; energy recovery; nutrient recovery; response surface optimization; biomass waste valorization; mechanistic understanding.

Broader context

Every year, three billion tons of agricultural and food wastes are produced in the U.S. Anaerobic digestion can partially convert such wastes into renewable biomethane while producing a lignocellulose- and nutrient-rich digestate coproduct that can lead to environmental problems due to improper land application. Hydrothermal liquefaction (HTL) provides an attractive option to convert digestate into marketable energy and nutrient-rich products. HTL research has focused, separately, on maximizing the energy or the nutrient recovery from biomass waste. To make HTL economically viable and more sustainable, simultaneous optimization of these parameters is required. These challenges motivated us to develop an experimentally informed mechanism for HTL of digestate that describes the main reaction pathways occurring in the bio-oil, aqueous, hydrochar, and mineral phases and their dependence on digestate compositions and process parameters. Using a structured experimental program, we provided a set of optimal HTL operating conditions for various digestate compositions that maximize bio-oil yield and quality and nutrient solubilization in the aqueous phase. Fundamental knowledge of thermochemical reaction pathways and mechanisms attributed to HTL of digestate presented in this article can help design and scale-up a more sustainable valorization process for agricultural and food wastes.

[a] *School of Chemical and Biomolecular Engineering, Cornell University, Ithaca, NY 14850*
[b] *Energy Systems Institute, Cornell University, Ithaca, NY 14850*
[c] *Chemical Engineering Department, Universitas Gadjah Mada, Yogyakarta 55281, Indonesia*
**Corresponding author*: hs987@cornell.edu
Electronic Supplementary Information (ESI) available: [details of any supplementary information available should be included here]. See DOI: 10.1039/x0xx00000x

1. Introduction

Widespread implementation of intensive industrial agricultural systems and accelerated development of refined food products to meet increasing global demand generates substantial wet biomass waste. For example, in the livestock cattle farming industry (including beef, dairy cows, and other types of cattle), approximately, 300 million tons of dry manure are produced annually (equivalent to ~3 billion tons of wet manure assuming an average 90% moisture content) from 94 million cattle raised in 882,692 cattle/calf farms in the U.S.[1] According to the Environmental Protection Agency's 2018 Wasted Food Report, approximately 103 million tons of food are wasted annually by the industrial, residential, institutional, and commercial sectors in the U.S.[2]

Anaerobic digestion (AD) including anaerobic co-digestion has been widely used to convert agricultural and food wastes into methane-rich biogas.[3] The biogas can be used for fuel, heat, and power generation, and can be injected into the natural gas grid after purification. Despite its advantages, AD produces a residual waste stream called anaerobic digestate – a wet mixture of organic and inorganic matrix rich in non-digested lignocellulosic fibers and nutrients whose compositions strongly depend on the characteristics of the substrates fed into the digester.[4]

Anaerobic digestate is commonly spread on agricultural fields and pastures and incorporated into the soil as an amendment/fertilizer. If mismanaged, this approach can potentially emit greenhouse gases,[5] form air-polluting ammonium aerosol salts,[4] cause phytotoxicity in plants,[6] spread pathogens,[7] and cause eutrophication and acidification in water basins due to N and P leaching and runoff from soil.[8] This calls for a more sustainable digestate management method, possibly in alignment with a circular bio-economy approach.

Hydrothermal liquefaction (HTL) is an attractive thermochemical process for the conversion of wet biomass waste (e.g., anaerobic digestates) into biocrude oil, a solid hydrochar, and an aqueous-phase (HTL-AP) coproduct. Compared to other thermochemical routes like pyrolysis and gasification, HTL is conducted in a pressurized liquid aqueous phase at temperatures above the boiling point of water but far below typical pyrolysis temperatures. Importantly, it does not require an energy-intensive pre-drying step.[9,10] HTL provides an activated environment for reformative chemistry in water near or above its critical temperature of 374°C. At near-supercritical conditions (280–360°C and 10–20 MPa), the dielectric constant of water decreases from 80 at 25°C to 15 at 360°C, and the ionic product of water (K_w) is on the order of 10^{-12} to 10^{-11} at 280-360°C, two to three orders of magnitude higher than that at 25°C (10^{-14}).[9] The lower water dielectric constant enables an easier solubilization of less-polar compounds, and its higher ionic product increases its ionic reactivity, making it both an acid and a base catalyst.

An important branch of HTL research has focused on maximizing biocrude yield and carbon content while minimizing its heteroatom (i.e., O and N) and nutrient (e.g., NH_3-N, P, K, Ca, and Mg) contents to facilitate coprocessing of HTL biocrude with conventional crude in petroleum refineries. The HTL temperatures between 310–350°C and the reaction times between 15–60 min have been reported to maximize biocrude yield and minimize biocrude heteroatoms content from a variety of feedstocks,[11–14] while homogeneous and heterogeneous catalysts have been reported to increase the carbon content in biocrude by catalyzing deoxygenation and denitrogenation reactions.[15–18]

Another branch of HTL research has instead focused on recovering nutrients from HTL products in the form of inorganic fertilizers, for example, struvite ($MgNH_4PO_4.6H_2O$) crystallization from the HTL-AP at alkaline conditions to produce a slow-release inorganic fertilizer providing plant-available P, N, and Mg.[19,26,27] To maximize struvite production from the HTL-AP, nutrients in the feedstock should preferentially partition in the HTL-AP, where they tend to assume their bioavailable forms (e.g., NH_4^+, orthophosphates, K^+, Ca^{2+}, and Mg^{2+}) rather than accumulate in the hydrochar phase in their non-bioavailable forms (e.g., apatite phosphate,[19] calcite,[20] and vivianite[21]). Since struvite formation is inhibited by the presence of Ca ions, Ca concentration in the HTL-AP should be minimized, as it would cause the formation of a more-thermodynamically-stable hydroxyapatite (a less effective P-fertilizer).[22] Increasing the HTL reaction temperature and/or reaction time have been reported to enhance the distribution of calcium and multivalent metals into the hydrochar and increase the NH_3-N yield in HTL-AP.[23] Moreover, pre-acidification of the feedstock to pH 2–4 maximizes N and P partitioning into HTL-AP.[19,24]

The feasibility and sustainability of HTL for sustainable resource recovery depends on the economic values and environmental benefits of the products generated. In this context, process conditions should be specified to simultaneously achieve the following targets: (1) maximum biocrude energy recovery, (2) low biocrude heteroatom content, (3) maximum yield of Mg, NH_3-N, and P in HTL-AP, and (4) minimum yield of Ca in HTL-AP. Specifying desirable HTL operating conditions requires a detailed understanding of the HTL reaction mechanisms, particularly those associated with the interaction between feedstock compositions and HTL operating conditions and their combined effects on HTL products.

The aim of this study is therefore twofold. The first is to provide a comprehensive mechanistic understanding of the combined effects of feedstock characteristics and process parameters on the final HTL products for digestate. The second is to establish a method for determining the HTL operating conditions that maximize energy and nutrient recovery based on various feedstock composition. These two key goals are achieved through the following five steps:

1. Preparation of a set of synthetic anaerobic digestate mixtures with different compositions (pH, salt content, and cellulose-to-lignin ratio).
2. Design of an HTL experiment matrix using a response surface methodology (RSM) based on half-fractional central composite design (HFCCD) to describe the effects of digestate compositions and HTL process conditions (reaction temperature and time) on biocrude energy

recovery; biocrude heteroatom (N and O) content; and mineral nutrient yield particularly Mg, NH_3-N, P, and Ca in HTL-AP. A total of 32 HTL experiments were performed. The HTL products separation and characterizations methods included filtration, extraction, elemental analysis, GC-MS, XRD, and colorimetry. Quadratic regression models for the corresponding response variables are obtained by fitting the results of the experimental analysis.

3. Proposal of a comprehensive HTL mechanism for digestate based on the results of the statistical analysis of the experimental outcomes and the comparative literature study.
4. Application of a desirability function approach[25] to determine a range of HTL process conditions to achieve the optimization targets. The exponential desirability function approach translates the regression equations obtained from the response surface experiment to a value between 0 (undesirable) and 1 (desirable).[25] This value is obtained as the weighted (geometric) average of the contributions of each optimization target, and it gives an idea of how close a set of specific operating conditions leads to the desired overall outcomes.
5. Validation of the suggested HTL process conditions by the desirability function approach through additional replicated HTL experiments on different digestate compositions.

While this work deals with the optimization of the HTL-AP composition for maximum struvite production, it does not describe the struvite production as well as its optimization. A detailed investigation of struvite crystallization from HTL-AP will be given in the forthcoming paper.

2. Materials and Methods

2.1 Synthetic anaerobic digestate preparation

Typical physicochemical properties of anaerobic digestates are presented in, indicating a high variability of cellulose-to-lignin (Cel/Lig) ratio, mineral salt content, and pH. The model compounds used to prepare the synthetic anaerobic digestate mixtures, including the supplier, purity, and the reasons for their selections, are shown in Table 1. Pre-selected model compounds were mixed with ultrapure water (18.2 mΩ·cm), and their compositions in the mixture for each experiment can be found in the SI (see Table S1, ESI). In general, the total concentration of cellulose and lignin was fixed at 8 wt%, the total concentration of amino acid and ammonium salt was fixed at 3 wt% (with NH_3-N to $N_{organic}$ molar ratio of 3:1), and the salt content varied from 1 to 5 wt%. This resulted in a total solid loading of 12–16 wt% in the mixture. The estimated ash content on dry matter basis was 8–31% (see Table S1, ESI), which falls within the reported values for ash content of anaerobic digestate.[26]

Table 1. Typical anaerobic digestate compositions and rationales for pre-selected model compounds to prepare synthetic anaerobic digestate mixture.

Typical digestate compositions from literature		Model compounds for synthetic digestate preparation	
Parameters	Ranges	Model Compounds	Rationales
Dry matter (DM), wt%	1.5-23.2[4,26]	Ultrapure water (Milli-Q water)	Used to adjust the dry matter content.
Organic, %DM Cel/Lig, g/g Total-C, %DM	60-80[26] 0.22-1.71[4,27] 26-45[4,26,28]	Alkaline lignin (≥94% purity, SCBT) Microcrystalline cellulose (≥99.99% purity, MiliporeSigma)	50-80% of organics in anaerobic digestate are non-digested lignocellulosic fibers.[4]
Total-N, %DM Org-N, %Total-N NH_3-N, %Total-N	2.4-7.6[4,28] 17.5-24.6[4,28] 55.4-82.5[4,28]	Glutamic acid (≥99.99% purity, BioBasic) NH_4-acetate (≥99.99% purity, J.T. Baker)	Org-N is from amino acids (protein hydrolysis).[4] NH_4^+ is very likely to chelate acetate produced from acidogenesis step.[26]
Ash, %DM P, %DM Ca, %DM Mg, %DM K, %DM	15-36[26] 0.6-1.7[26] 1-2.3[4,26] 3-7[4,26] 1.2-11.5[4,26]	$CaHPO_4.2H_2O$ (≥99% purity, Eisen-Golden) $CaCO_3$ (≥99% purity, Loudwolf) $MgCO_3$ (≥98% purity, Aldon Corp.) KCl (≥99.99% purity, EMD Chemicals)	P existed mostly as $CaHPO_4.2H_2O$ in the digestate.[29] Ca and Mg existed as $CaCO_3$ and $MgCO_3$, respectively, from the reaction with CO_3^{2-}.[26,30] K exists as soluble halide salts in the digestate.[26]
pH	7-9[4,26]	Acetic Acid (≥99.5% purity, J.T. Baker) NaOH (100% purity, Belle Chemical)	Acetic acid is used for acidification as it is the primary product from acidogenesis.[26] NaOH is used to control pH in digesters.[30]

2.2 HTL procedure and product analysis

The HTL experiments used the same experimental setup and procedures as described in a previous study by our group in Figure S1 (ESI).[20] With this setup, the heating time required to reach the target reaction temperature of 280, 300, 320, 340, and 360 °C were around 45, 50, 60, 70, and 80 min, respectively (see Figure S19, ESI). Meanwhile, the cooling time required to reach ~80 °C (where no hydrothermal reaction takes place) was consistently around 15 min (see Figure S19, ESI). The statistical analysis shown in Table S15 and S16 (see ESI) indicates that the effects of the experimental variation of the heating and cooling time due to the system setup was statistically insignificant on the HTL outcomes, compared to the effect of the other studied process parameters. Therefore, this experimental design provides an appropriate structure for the central composite design to efficiently evaluate the effects of important variables within their realistic operating ranges.

Three products were collected from each experiment: biocrude oil, hydro-char, and HTL-AP. Three biocrude extraction fractions were collected: dichloromethane-extracted and ethyl-acetate extracted water-soluble biocrudes (DWO and EWO), and dichloromethane-extracted solid-bound biocrude (DSO). The yield of biocrudes or hydrochar was calculated using Eq. 1. The ash content in biocrudes was determined with the ASTM E1131-20 method[31] to obtain the dry-ash-free yield of biocrude (see Eq. 2). The total biocrude oil yield was calculated as the sum of the yield of DWO, EWO, and DSO extraction fractions. The elemental content ($\%C_i$, $\%H_i$, $\%N_i$, and $\%O_i$) of biocrudes and hydrochar was measured with a CE-440 Elemental Analyzer (Exeter Analytical). The biocrude higher heating value (*HHV*) was calculated according to the elemental composition using the equation by Channiwala and Parikh,[32] and the total energy recovery was calculated with Eq. 3.

$$Y_i = \frac{m_i}{m_{feedstock}} \times 100\% \quad (1)$$

$$Y_{oil,daf} = \frac{m_{oil} \times (1 - \%Ash_{oil})}{m_{feedstock}} \times 100\% \quad (2)$$

$$ER_{oil} = \frac{m_{oil} \times HHV_{oil}}{m_{feedstock} \times HHV_{feedstock}} \times 100\% \quad (3)$$

Y is the product mass yield, *m* is the product mass (g), *i* indicates biocrude oil or hydrochar, $m_{feedstock}$ is the dry mass of feedstock (g), $Y_{oil,daf}$ is the dry-ash-free mass yield of biocrude, m_{oil} is the biocrude mass (g), $\%Ash_{oil}$ is the ash content of biocrude (wt%), and ER_{oil} is the biocrude energy recovery.

The yield of carbon and nitrogen in biocrude or hydrochar was calculated using Eq. 4, while their yield in HTL-AP were calculated using Eq. 5 and 6.

$$X_{yield-i} = \frac{(\%X_i) \times m_i}{X_{feedstock}} \times 100\% \quad (4)$$

$$C_{yield-AP} = \frac{[TOC]_{AP} \times (V_{AP})}{X_{feedstock}} \times 100\% \quad (5)$$

$$N_{yield-AP} = \frac{[TN]_{AP} \times (V_{AP})}{X_{feedstock}} \times 100\% \quad (6)$$

X_{yield} represents the mass yield of carbon or nitrogen, $\%X_i$ is the elemental content of carbon or nitrogen in biocrude or hydro-char, *i* indicates biocrude or hydrochar, and $X_{feedstock}$ is the mass of carbon or nitrogen in the feedstock (g). The total yield of carbon and nitrogen in biocrude ($C_{yield-oil}$ or $N_{yield-oil}$) is the sum of carbon or nitrogen yield in the three biocrude extraction fractions. Meanwhile, $C_{yield-AP}$ and $N_{yield-AP}$ are the yield of carbon and nitrogen, respectively, in HTL-AP, $[TOC]_{AP}$ and $[TN]_{AP}$ are the total organic carbon and the total nitrogen concentration (mg/L), respectively, measured using a Shimadzu TOC-L CSN, and V_{AP} is the HTL-AP volume (L).

The nutrient concentration in HTL-AP ($[X]_{AP}$, mg/L) was measured colorimetrically (Hanna Instruments HI83399). NH_3-N, P, K, Cl, Mg, and Ca were determined with the ASTM D1426−15,[33] amino acid,[34] tetraphenylborate,[35] mercury (II) thiocyanate,[36] Calmagite,[37] and oxalate[38] methods, respectively. The nutrient yield in HTL-AP (Z_{AP}) was calculated with Eq. 7 based on colorimetrically-measured nutrient concentration ($[Z]_{AP}$, mg/L – using HI83399 photometer from Hanna Instruments) where *Z* represented any one of NH_3-N, P, Mg, and Ca, V_{AP} is the HTL-AP volume, and $Z_{feedstock}$ is the mass of *Z* in the feedstock (g).

$$Z_{AP} = \frac{[Z]_{AP} \times V_{AP}}{Z_{feedstock}} \times 100\% \quad (7)$$

The yield of nutrient (*Z* – Mg, P, or Ca) in the hydrochar (Z_{HC}) was calculated using Eq. 8 where $\%Z_{HC}$ is the nutrient content of the hydro-char measured using energy dispersive X-ray spectroscopy (Oxford Instruments)

$$Z_{HC} = \frac{\%Z_{HC} \times m_{HC}}{Z_{feedstock}} \times 100\% \quad (8)$$

GC-MS compositional analysis (Agilent 6890N GC with a JEOL JMS-GCMATE II MS) was performed on selected biocrude samples (GC-MS operating conditions and procedure are given in Table S6, ESI) to semi-quantify the presence of organic compounds. The thermogravimetric analysis (TGA) was also performed by heating 10–20 mg of selected biocrude samples from room temperature to 700°C at 10 °C/min in 50 mL/min of atmospheric nitrogen (TA Instruments QA500). The TGA results given in Figure S20–S21 (ESI) showed that 60–80% components in the biocrude samples have boiling point ≤300°C; thus, majority of chemical compounds in the biocrude were detectable using the adopted GC-MS procedure.

The HTL-AP was also analyzed for the organic compositions with GC-MS, which was performed similarly to that for biocrude with pre-derivatization following the methyl-chloroformate method.[39] In addition, the liquid-phase product was measured for pH to determine pH change after reaction (ΔpH_{liq}). To investigate the phase transformation of precipitated mineral nutrients, the hydrochar mineral compositions were characterized with XRD (Bruker D8 Advance ECO).

2.3 Structure of the Experiments and Modelling

Design of experiments

A composite design following the HFCCD protocol[40] was adopted to explore all combinations of independent variables

Table 2. Simple design matrix for HTL experiments[40]

Independent variables	Factor levels				
	-2	-1	0	1	2
X_1. Reaction temperature (°C)	280	300	320	340	360
X_2. Reaction time (minute)	10	20	30	40	50
X_3. Feedstock pH	2.5	4	5.5	7	8.5
X_4. Salt content (wt%)	1	2	3	4	5
X_5. Cel/Lig ratio	0.2	0.6	1	1.4	1.8

systematically and practically, i.e., reaction temperature and time, feedstock pH, salt content, and cellulose-to-lignin ratio. The HFCCD is constructed on a two-level (factor level -1 and 1) half-factorial design added with a center point (factor level 0) and a group of axial points (factor level -2 and 2), making each factor has five levels. To investigate the five independent variables in this study, the HFCCD generated thirty-two sets of HTL experiments (see full design matrix in Table S2, ESI) comprising sixteen half-factorial points, ten axial points, and one five-time-replicated center point to assess reproducibility.

The selected ranges for the investigated operating conditions (see Table 2) were selected to gain mechanistic understandings of the elemental distribution in the major products. Reaction temperatures of 280–360°C were chosen because this range has been reported to produce the highest biocrude and nutrient yields.[41] Reaction times of 10–50 min were selected as this range has been reported to provide a total conversion of biomass.[41] The selected ranges for feedstock compositional parameters cover the typical physicochemical properties of anaerobic digestates (see

Table 1). The range for feedstock pH was determined according to the typical pH of anaerobic digestate (pH 7–9, see

Table 1) and the preferred pH for acidic depolymerization of lignin (pH 2–6).[42] The range for salt content and Cel/Lig ratio were based on the reported values for various anaerobic digestates (see

Table 1). Data on measured responses (see the response variables in subsection 2.2) were fitted with a quadratic regression equation (see Eq. 6)[40] with independent variables standardized on the factor level scale (coded units).

$$F = \alpha_0 + \sum_{i=1}^{n} \alpha_i X_i + \sum_{i=1}^{n} \alpha_{ii} X_i^2 + \sum_{i=1}^{n-1} \sum_{j=i+1}^{n} \alpha_{ij} X_i X_j \qquad (6)$$

F is the response variable, α_0 is the constant, X is the independent variable, and α_i, α_{ii}, and α_{ij} are the coefficient of linear, quadratic, and interaction terms, respectively. The equations in coded units were statistically analyzed in Minitab 19.2.0. Only statistically significant factors/terms (p <0.05) were included in the equation. The model's adequacy was determined with R^2, R^2(pred.), and lack-of-fit p-value.

Multi-response optimization based on the generated regression equations was performed in Minitab 19.2.0 using the desirability function approach.[25] For different salt contents and Cel/Lig ratios in the digestate, the desirability function approach computed the optimal values of the independent variables (reaction temperature, reaction time, and feedstock pH) that can achieve the optimization targets: (1) maximum biocrude energy recovery, (2) low biocrude heteroatom content, (3) maximum yield of Mg, NH_3-N, and P in HTL-AP, and (4) minimum yield of Ca in HTL-AP. All targets were given an equal weighting factor because we assumed that both biocrude and nutrient-rich HTL-AP have the same potential economic values and environmental benefits. To validate the accuracy of this procedure, synthetic anaerobic digestates with four different compositions covering the whole spectrum of the optimization were processed using the computed optimum HTL process conditions in five-time-replicated HTL experiments. Both experimental and predicted (using the regression equations) results of the response variables obtained for each digestate composition were compared.

Treatment of Experimental Results and Mechanistic Modelling

The presentation of the results of our study are divided into two parts: (i) An experimental-based HTL mechanism and (ii) Optimization and validation of HTL operating conditions. The first part describes the combined effects of digestate characteristics and HTL parameters on the final products and proposes comprehensive HTL reaction mechanisms for digestate. This part relies on the results of the statistical analysis of the response variables and on their comparison with the available literature to draw mechanistic understandings. The second part deals with the optimization of HTL conditions based on digestate composition with the aim of maximizing energy and nutrient recovery. The validation of the proposed approach through additional HTL tests is also presented in the second part.

3. Experimental-Based HTL mechanism

This section discusses the effects of the independent variables on the d.a.f. oil yield, heteroatom content in DSO (dichloromethane-extracted solid-bound biocrude) and DWO (dichloromethane-extracted water-soluble biocrude) biocrude products, and nutrient yield in HTL-AP. This is done through a regression analysis of the experimental results from the thirty-two runs in the HTL experiment matrix, providing regression equations for all the independent variables.

In order to allow the reader to compare the relative influence of each independent variable on the response variables, Table 3 collects the coefficients for each significant term in the equations for all response variables (Eq. 6) including the statistics, i.e., R^2, R^2(pred.), and the lack-of-fit p-value. The coefficients refer to the coded units (standardized variables), thus allowing a direct comparison of the coefficients. The p-values for each significant term are reported in Table S3-S5 (ESI). Furthermore, to show the response variable's critical points (e.g., maxima, minima, or saddle point) as functions of the independent variables, representative contour plots are presented in the following subsection. These plots are obtained

Table 3. Regression coefficients (truncated to three decimal places) for all measured response variables (see Table S3-S5 in ESI for untruncated coefficient values and a complete statistical assessment of the regression models).

Terms	Measured Response Variables											
	$Y_{oil,daf}$ (%)	$C_{yield\text{-}oil}$ (%)	ER_{oil} (%)	ΔpH_{liq}	$\%O_{oil\text{-}DWO}$	$\%O_{oil\text{-}DSO}$	$\%N_{oil\text{-}DWO}$	$\%N_{oil\text{-}DSO}$	$NH_3\text{-}N_{AP}$ (%)	P_{AP} (%)	Mg_{AP} (%)	Ca_{AP} (%)
Constant	40.063	69.46	66.463	-0.566	60.341	22.892	0.879	2.115	34.298	17.027	64.540	32.416
T	2.390	5.789	6.577	-0.033	-2.705	-1.324	-0.026	0.058	-0.878	0.766	1.540	-1.917
t	-	-	1.658	-0.021	-1.299	-1.125	0.004	0.029	-0.584	-0.33	-0.750	-0.670
pH	-6.664	-8.94	-9.529	-0.491	-0.522	-1.600	0.087	0.373	-4.332	-12.673	-11.804	-8.552
Salt	-4.883	-4.272	-4.034	0.194	-0.947	-0.844	0.145	0.025	-	-5.807	-6.620	-2.523
Cel/Lig	1.508	3.96	3.377	-0.204	-0.187	-1.590	0.014	0.237	-2.924	5.708	-	2.331
T^2	-1.188	-2.305	-2.090	-0.099	-	-	-0.06	-0.257	2.687	-	-5.364	-
t^2	-	-	-	-	-	-	-0.057	0.244	2.110	-	-2.540	-
pH^2	-6.254	-11.636	10.852	0.143	1.215	0.867	-	-	1.041	7.624	-	-1.773
$Salt^2$	-	-	-	-	-	-	0.018	0.207	-	-	-	-
Cel/Lig^2	-	-	-	-	-	-	-	-	-2.219	-	-	-
T×t	-	-	-	-	-0.112	-0.813	-	-	-1.453	2.677	-	2.218
T×pH	-	-	-	-	-	-	-	-	1.910	-	-	-
T×Salt	-	-	-	-	-0.224	-0.838	-	-	-	-	-	-
t×pH	-	-	-	-	0.016	0.798	-	-	-	-	-	-
t×Cel/Lig	-	-	-	-	0.448	0.959	-	-	-	-	-	-
pH×salt	-	-	-	-	-	-	0.002	0.036	-	4.984	7.794	-1.988
pH×Cel/Lig	1.461	2.360	-	-0.213	0.284	1.083	-	-	-	-4.805	-	-
Salt×Cel/Lig	-	-	-	-	0.250	0.779	-	-	-	-4.609	-	-2.222
R^2	97.59%	94.68%	96.07%	89.41%	83.44%	85.63%	90.01%	99.14%	89.51%	97.49%	89.77%	93.53%
R^2(pred.)	93.57%	88.31%	91.00%	73.92%	75.29%	76.55%	65.98%	97.48%	67.58%	93.21%	79.29%	80.21%
Lack-of-fit's *p*-value	0.173	0.190	0.300	0.206	0.335	0.363	0.340	0.452	0.505	0.254	0.385	0.085

by varying two statistically significant variables in the regression equations and keeping the other variables constant at factor level zero (see the natural value of factor level zero in Table 2). A complete list of the plots is reported in Figure S2-S12 (ESI).

Based on the statistical analysis of the experimental results and the comparison with the literature, we proposed comprehensive HTL reaction pathways for anaerobic digestate that are summarized in Figure 1. Each reaction pathway in Figure 1 is labelled using the convention ***r#***, where **#** is the reaction code. When a reaction pathway is discussed in the following subsections, the code is placed next to the corresponding text to allow an easier referencing to Figure 1.

The proposed reaction pathway for the conversion of organics focused on the chemical compound formation in the biocrude and aqueous-phase products, which accounted for 55.9–95.2% of the overall mass balance, 60.2–96.0% of the carbon balance, and 54.4–92.1% of the nitrogen balance. Similarly, the proposed distribution pathway for the inorganics focused on their partitioning between hydrochar and the aqueous-phase coproduct since 95.52–99.75% of P, 97.19–99.75% of Ca, and 94.81–99.87% of Mg in the digestate were distributed into these two product phases. Comprehensive mass and elemental balances are shown in Table S10, S11, S12, S14, and S17 in the ESI.

3.1 D.a.f. oil yield

The measured total oil yield was 7.03–55.80% with an ash content of 1.51–9.71%; the d.a.f. oil yield was 5.52–51.80%. Among the three biocrude extraction fractions, DSO contributed 60-80% of the d.a.f. oil yield ($Y_{oil,daf}$), followed by DWO 20–35% and EWO <5%. The carbon yield in biocrude ($C_{yield\text{-}oil}$) varied between 9.23–54.8%, 1.21–19.24%, and 0.27–13.82% for DSO, DWO, and EWO biocrude fractions, respectively, resulting in total energy recovery (ER_{oil}) of 10.1–76.1%. The HHV of biocrudes ranged between 15 and 32 MJ/kg, similarly to previously reported values.[43,44] From the coefficient of each term in the regression model of $Y_{oil,daf}$, $C_{yield\text{-}oil}$, and ER_{oil} (see Table 3), all factors except reaction time had similar effects on these three response variables, thus indicating that the amounts of carbon and energy recovered were strongly associated with the amount of biocrude oil produced. For comprehensive understandings of the effects of the statistically significant factors (p <0.05) on biocrude production, reaction mechanisms based on chemical compositions in the biocrude are discussed, with a focus on the DSO and DWO fractions because of their major contributions to $Y_{oil,daf}$.

Effect of feedstock pH

Feedstock pH was the most significant factor for biocrude

formation as indicated by the largest coded coefficient of its linear and quadratic term (see Table 3). In general, a more acidic

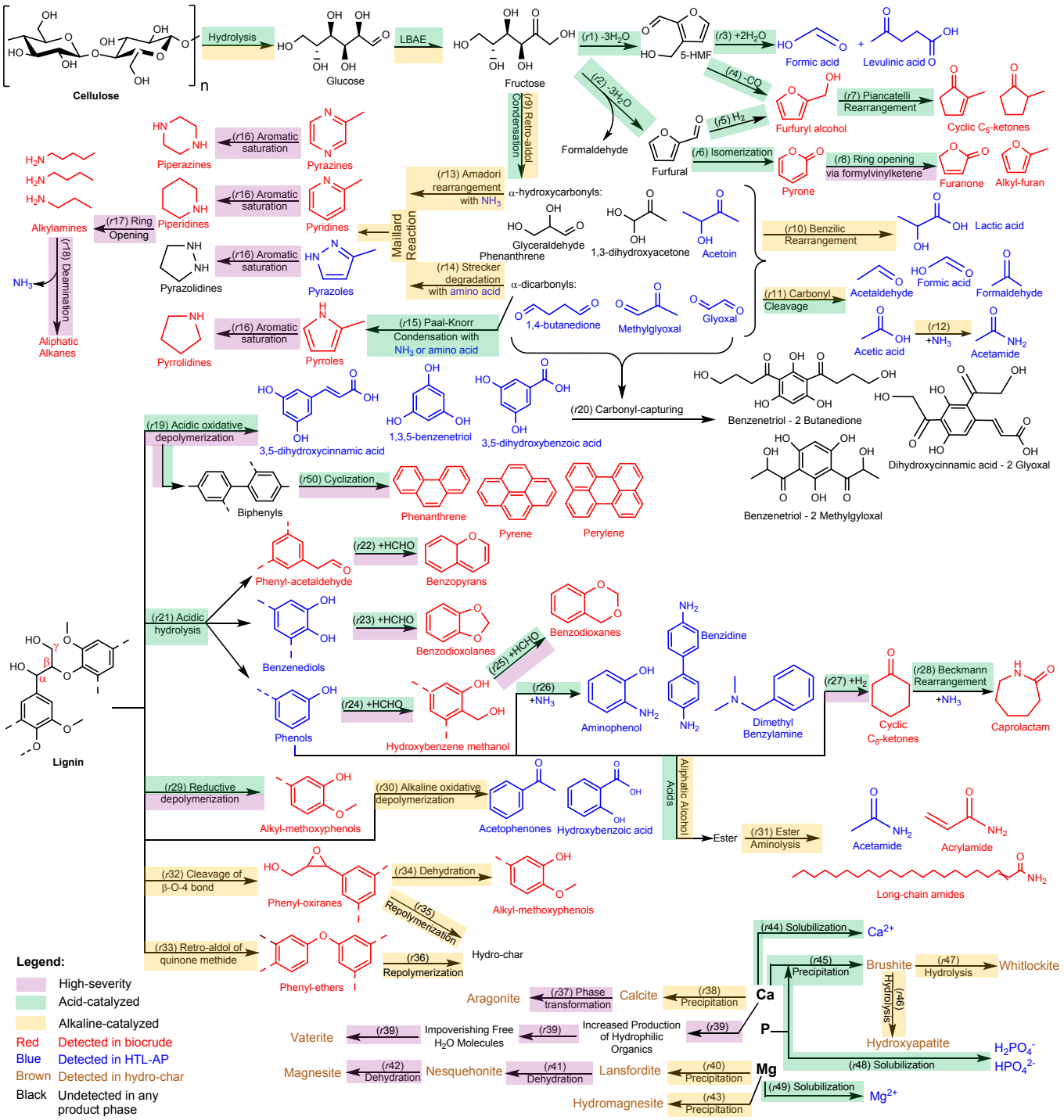

Figure 1. Proposed reaction mechanism for HTL showing the major reaction pathways of organics and inorganics during HTL of synthetic anaerobic digestate. Each reaction pathway is labelled using ***r#***, where **#** is the reaction code. The chemical structures were created using ChemDraw 20.1.1.

feedstock produced a higher $Y_{oil,daf}$, and the yield was highest at pH around 5 (Figure 2-B). Under acidic conditions, carbohydrate monomers produced from cellulose hydrolysis were substantially converted via dehydration into furfural (***r2***) or 5-HMF (***r1***). The furfural pathway comprised isomerization (***r6***) and ring-opening (***r8***) or hydrogenation (***r5***) and Piancatelli rearrangement (***r7***) of furfural[45,46] to produce pyrones, cyclic ketones, and furanones, which were dissolved in the biocrude product-phase (see Table S7, ESI). The 5-HMF pathway can produce the same products as the furfural pathway via decarbonylation of 5-HMF[47] (***r4***) followed by Piancatelli rearrangement (***r7***). However, the presence of levulinic acid and formic acid in HTL-AP produced from acidic feedstocks (see Table S8, ESI) showed that rehydration of 5-HMF (***r3***) also occurred. Because both decarbonylation (***r4***) and rehydration (***r3***) of 5-HMF are acid-

catalyzed and can occur concurrently,[48] the maximum $Y_{oil,daf}$ at a feedstock pH of ~5 indicated the optimum feedstock pH at which the selectivity for 5-HMF rehydration was lowest. This result is in accordance with previous studies reporting that 5-HMF rehydration

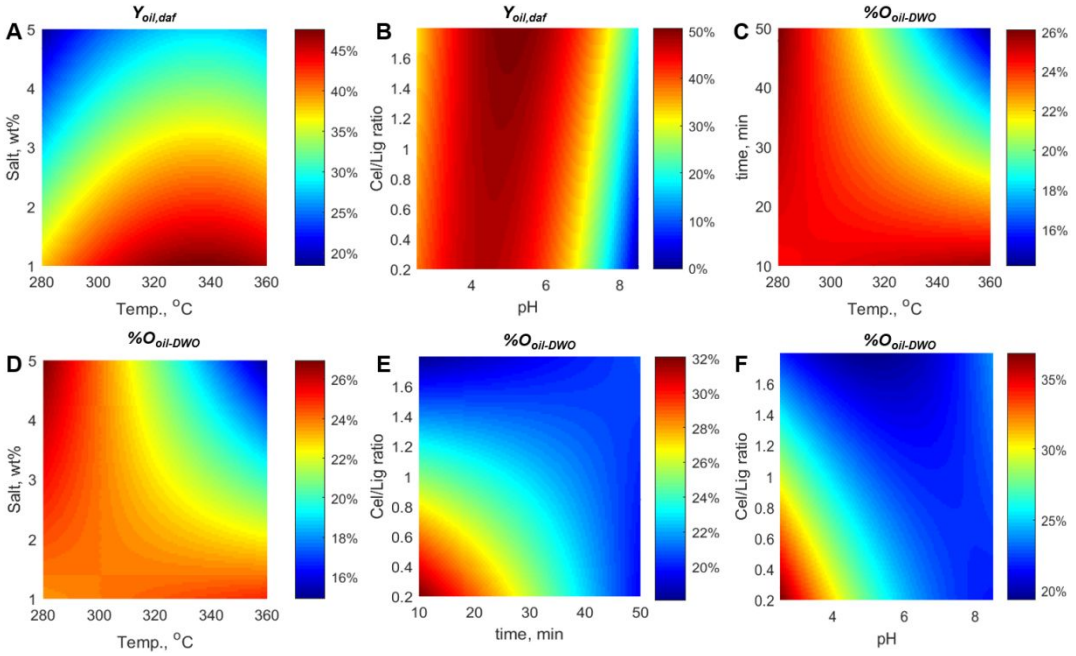

Figure 2. Representative contour plots of d.a.f. oil yield ($Y_{oil,daf}$, A–B) and biocrude (DSO) oxygen content ($\%O_{oil}$, C–F).

in subcritical water is expedited at pH <5,[49] and was further validated by chromatography analysis of HTL-AP produced from feedstocks with pH 2.5 and 5.5 (see Table S8, ESI). A larger peak area percentage of levulinic acid and formic acid was observed at a feedstock pH of 2.5.

Although 5-HMF rehydration is inevitable and undesirable from an energetic perspective, the formic acid produced in this reaction might be beneficial in preventing repolymerization of lignin monomers. During acidic treatment, lignin undergoes depolymerization (e.g., acidolysis) into oil and water-soluble monomers and repolymerization into a char-like precipitate.[50] Reductive depolymerization of lignin (***r*29**) with formic acid as a hydrogen donor may block the repolymerization and increase the $Y_{oil,daf}$ from lignin via hydrogenolysis of interunit β-O-4 and α-O-4 ether bonds and removal of benzylic OH-groups to produce alkyl-substituted methoxyphenols.[42,51] In addition, phenolic monomers produced from lignin acidolysis (***r*21**) may also benefit from the presence of hydrogen donors, which allows their conversion into cyclic C_6-ketones (***r*27**).[52] Both alkyl-substituted methoxyphenols and cyclic C_6-ketones were non-polar and dissolved in the biocrude product-phase (see Table S7, ESI), and their production has been found to increase $Y_{oil,daf}$.[42]

Phenolic compounds with a hydroxymethyl, a dioxane/dioxolane, and a pyran structure were observed in the biocrudes produced from acidic feedstocks, e.g., 4-hydroxy-benzenemethanol, 1,3-benzodioxane-5-ol, 5-(1-propenyl)-1,3-benzodioxole, and 3,5,7-trihidroxy-benzopyranone (see Table S7, ESI). The presence of a hydroxymethyl group suggests that a sufficient amount of formaldehyde readily attacked and deactivated reactive sites of the aromatic rings during the reaction (***r*24**).[53,54] The formaldehyde may originate from lignin side chain cleavages during lignin acidolysis and the fragmentation of monosaccharides via acid-catalyzed retro-aldol reactions.[53,55] The presence of dioxane/dioxolane and pyran structures indicated stabilization of lignin monomers (i.e., C_2-aldehyde-substituted phenols and Hibbert's ketones) by the formation of cyclic acetal (***r*23** and ***r*25**) and pyran (***r*22**) from the reaction between formaldehyde and the hydroxyl/ketone group of alkyl side chains on the phenyl ring.[42,54] Stabilization through hydroxymethylation and the formation of cyclic acetal and pyran restrained the repolymerization of lignin-derived biocrude into solid hydro-char, thus producing higher $Y_{oil,daf}$.

Effect of reaction temperature

A quadratic dependence of $Y_{oil,daf}$ was also observed on the reaction temperature although it was statistically less significant than feedstock pH (smaller coefficient value in Table 3). Raising the reaction temperature from 280°C to 330°C increased the $Y_{oil,daf}$ (Figure 2-A); thus, high reaction temperatures were required to thermochemically breakdown the recalcitrant cellulose and lignin. Moreover, high reaction temperature promoted oxidative degradation (***r*19**) of lignin into biphenyls, which can experience cyclization and dehydration (***r*50**) to form polyaromatic compounds,[56] such as phenanthrene, pyrene, and perylene, in biocrude phase. These non-polar polyaromatic compounds are reported to be the precursor of high boiling point compounds that are similar to those found in conventional crude oil.[57] Indeed, TGA analysis of

selected biocrude samples (see Figure S20 and S21 in the ESI) show that 20 – 40% of the oil has boiling point ≥ 300°C. Nevertheless, a further increase in HTL temperature (>330°C)

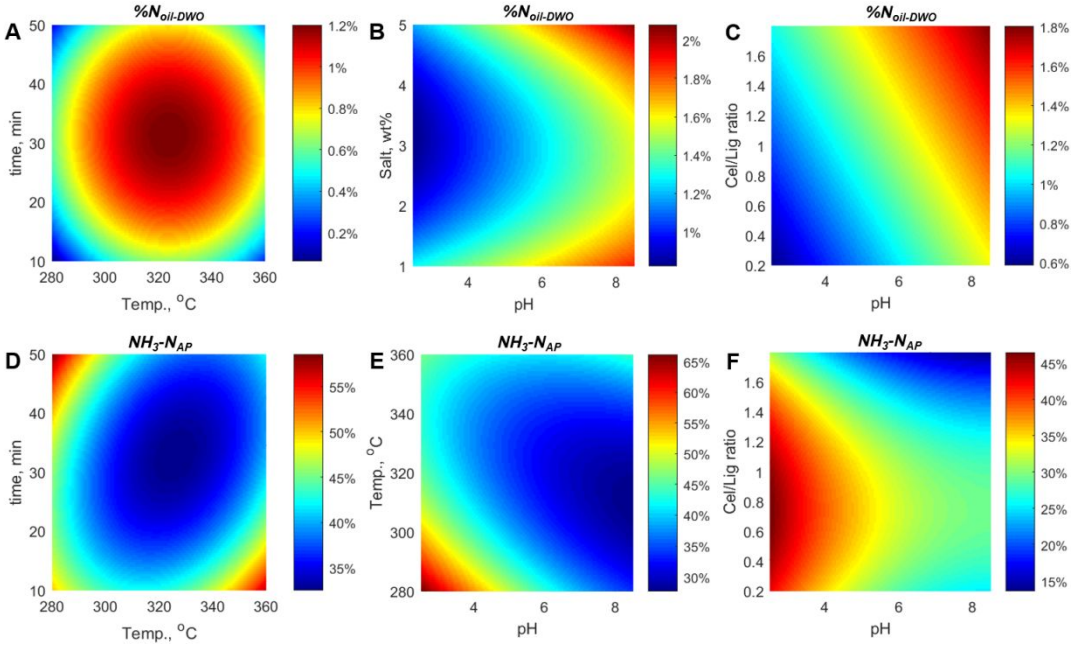

Figure 3. Representative contour plots for biocrude nitrogen content ($\%N_{oil}$) in DWO biocrude fractions (A-C) and NH_3-N yield in HTL-AP (D-F).

gradually decreased the $Y_{oil,daf}$, owing to partial thermal-oxidative fragmentation of biocrude components into gas.[58] In addition, repolymerization of components in lignin-derived biocrude into solid hydro-char may also occur due to faster decomposition of lignin-stabilizing agents (e.g., formaldehyde) above 330°C.[59]

Effect of salt content

A higher salt content decreased the $Y_{oil,daf}$ (negative linear coefficient in Table 3). Salt in the digestate comprised mostly carbonate minerals (e.g., $CaCO_3$ and $MgCO_3$) and higher carbonate mineral concentrations may increase feedstock alkalinity (positive linear effect of salt content on ΔpH_{liq}, see Table 3) and direct cellulose and lignin decomposition toward the alkaline pathway. Alkaline-catalyzed retro-aldol condensation (***r*9**), benzilic acid rearrangement (***r*10**), and carbonyl cleavage (***r*11**) convert cellulose into aqueous organics, such as lactic acid, acetaldehyde, acetic acid, and acetoin (see Table S8, ESI), leading to a lower $Y_{oil,daf}$.[55] Moreover, alkaline-catalyzed lignin degradation transformed phenolic units into quinone methides and non-phenolic units into phenyl-oxirane intermediates (***r*32**),[60,61] both of which are prone to condensation into hydro-char (***r*35** and ***r*36**).[62] Enol-ethers (the products of retro-aldol decomposition of quinone methide, ***r*33**) and phenyl-oxiranes were present in the biocrudes produced from alkaline (pH 8.5) and high-salt-content (5wt%) feedstocks (Table S10, ESI). In addition, alkaline conditions also converted lignin into aqueous acetophenone and hydroxybenzoic acids (***r*30**) according to Table S8 (ESI).

Effect of cellulose-to-lignin ratio (Cel/Lig)

The presence of more lignin in the digestate inhibited the biocrude formation (positive linear coefficient of Cel/Lig for $Y_{oil,daf}$ in Table 3). This inhibition may be associated with the susceptibility of lignin degradation products to recondensation into hydro-char.[63] Despite previous works reported restricted accessibility of cellulose due to lignin-cellulose complex formation for biomass waste as a cause for lower biocrude production,[64] this is unlikely to be true for synthetic anaerobic digestate as lignin and cellulose were supplied as unbound pure components in the mixture. The negative effect lignin has on $Y_{oil,daf}$ can be mitigated by employing slightly less acidic feedstock pH (pH 4–5, see Figure 2-B) due to the positive interaction between feedstock pH and Cel/Lig (see Table 3).

3.2 Heteroatom content in biocrudes

Oxygen content

The oxygen content in the biocrudes ($\%O_{oil}$) for all the experiments was 18.2–36.4% for DSO (dichloromethane-extracted solid-bound biocrude) and 29.7–43.7% for DWO (dichloromethane-extracted water-soluble biocrudes) – values higher than those in conventional crude oils.[65] However, the regression models for $\%O_{oil\text{-}DWO}$ and $\%O_{oil\text{-}DSO}$ (see Table 3) revealed that the process conditions can be tailored to ensure HTL of anaerobic digestate produces biocrudes with the lowest possible oxygen content. High reaction temperatures and long

reaction times decreased the oxygen content (see Figure 2-C), as indicated by the negative linear coefficients emphasizing negative interactions between factors (see Table 3). Specifically, reaction temperatures >310°C and reaction times >30 min are recommended for feedstock with salt content >2wt% and Cel/Lig >1.2, respectively (Figure 2-D and Figure 2-E). Increasing the feedstock pH also significantly decreased the $\%O_{oil}$ with a plateau starting at pH ~6. For digestates containing Cel/Lig >1.5, feedstock pH >6 is not recommended because the oxygen content in biocrudes would slightly increase through the positive interaction of pH with Cel/Lig (Figure 2-F). These suggested process conditions were associated with decarboxylation (mostly in DSO) and dehydration (mostly in DWO) reactions, according to the Van Krevelen diagrams of different biocrude fractions shown in Figure S13-S14 (ESI).

Nitrogen content

The nitrogen content in biocrudes obtained for all experiments varied between 2.1-5.4% for DWO and 1.0-3.1% for DSO. These levels exceed concentrations found in most conventional crude oil (0.25%).[66] From the regression equations for $\%N_{oil\text{-}DWO}$ and $\%N_{oil\text{-}DSO}$ (see Table 3), feedstock pH was identified as the most important factor with a positive linear effect on biocrude nitrogen content ($\%N_{oil}$). This effect can be explained considering that at a higher feedstock pH (more alkaline), cellulose degradation proceeded mostly through the alkaline pathway and produced electrophilic α-dicarbonyl and α-hydroxycarbonyl compounds (e.g., glycolaldehyde, hydroxybutanone, methylglyoxal, and glyoxal (***r*9**); see Table S8, ESI), which are more reactive intermediates than reducing sugars for the Maillard reaction.[67] In addition, alkaline conditions increased the nucleophilicity of amino group of amino acids and ammonia, enhancing the Maillard reaction by forming aminocarbonyl intermediates through Strecker degradation of amino acids with the help of α-dicarbonyls (***r*14**)[68] and Amadori rearrangement of ammonia with α-hydroxycarbonyls (***r*15**).[69] Pyridines, pyrazines, azoles, pyrroles, and their derivatives (see Table S7, ESI) were observed as products of Maillard reaction (aromagenic pathways),[70,71] and the presence of amides (e.g., 9-octadecenamide and 13-docosenamide) indicated that base-catalyzed ester aminolysis (***r*31**) also contributed to nitrogen fixation in biocrude.[72]

From the above explanations, low-pH feedstocks (acidic) can achieve lower $\%N_{oil}$, because the Maillard reaction is inhibited. However, chemical compounds similar to Maillard reaction products, i.e., caprolactam and pyrroles, still existed in biocrudes produced from acidic feedstocks (see Table S7, ESI). Because the Maillard reaction is inhibited under acidic conditions, two potential alternative reaction mechanisms are Beckmann rearrangement (***r*28**, cyclic C_6-ketones conversion into caprolactam)[73] and Paal-Knorr condensation (***r*15**, pyrroles formation from the reaction between 1,4-dicarbonyl compounds with amino-acid or ammonia),[74] both of which are acid-catalyzed. Detailed mechanisms have been described in the literature.[73,74]

The $\%N_{oil}$ showed quadratic dependence on reaction temperature and time (see Table 3), yielding global maxima at 330°C and 30 min (Figure 3-A). Therefore, lower temperatures coupled with shorter reaction times (milder conditions) and higher temperatures coupled with longer reaction times (more-severe conditions) can produce low $\%N_{oil}$. The milder conditions decreased $\%N_{oil}$ because reactions generating less polar N-heterocyclic compounds, such as the Maillard reaction, Paal-Knorr condensation, and ester aminolysis, were not fully activated at these conditions. Meanwhile, the higher temperatures and longer reaction times allowed the hydro-denitrogenation reaction to occur, removing nitrogen from biocrudes. The course of hydro-denitrogenation reactions in the high-severity process was demonstrated by an increase in peak area percentages of saturated heterocyclic amines, alkylamines, and alkanes in the biocrudes (see Table S7, ESI). The increased detection of piperidines, piperazines, and pyrrolidines indicated the aromatic saturation (***r*16**) of pyridines, pyrazines, and pyrroles, respectively. Aromatic saturation is critical to facilitate ring-opening (***r*17**) by converting the hybridization state of carbons surrounding the C-N bond to sp^3 to obtain a weaker bond dissociation energy. The increased detection of alkylamines and alkanes (C_4-C_5) indicated that the saturated aromatic rings of piperidines, piperazines, and pyrrolidines were opened via C-N bond cleavage, followed by deamination via Hoffmann elimination or S_N2-type substitution, releasing alkanes and NH_3 as a byproduct (***r*18**).[66,75,76]

Increasing the feedstock cellulose-to-lignin ratio had a positive linear effect on $\%N_{oil}$ (see Table 3, Figure 3-C); in other words, a lower ration, with higher lignin content than cellulose, suppressed nitrogen fixation in the biocrude. At lower Cel/Lig ratios, excess phenols or phenolic acids produced from the hydrothermal oxidative decomposition of lignin (***r*19**) may prevent cellulose-derived α-dicarbonyls/α-hydroxycarbonyls from participating in nitrogen-fixing reactions (e.g., Maillard reaction and Paal-Knorr condensation). The potential prevention mechanism involves the capture of the electrophilic carbon of the carbonyl group by the aromatic rings of phenols or phenolic acid through an ortho- or para-directed electrophilic aromatic substitution (***r*20**).[77] Although products of this mechanism, such as dihydroxycinnamic-acid-2-glyoxal and benzenetriol-2-butanedione, were not detected in biocrudes due to their non-volatile nature, several *meta*-hydroxyl-containing phenols (e.g., 3,5-dihydroxycinnamic acid, 1,3,5-benzenetriol, 5-tert-butylpyrogallol, and 3,5-dihydroxybenzoic acid) were detected with an increased extent in HTL-AP of lignin-rich feedstock (see Table S8, ESI). Since a *meta* configuration of the electron donor (-OH group) at carbons number 3 or 5 in the phenol ring has a higher reactivity toward carbonyl-capturing at the ortho or para position, their increased detection suggests the capturing reaction (***r*20**) has likely to occurred.[77]

Salt content had a quadratic effect on the $\%N_{oil}$ (see Table 3) with minima at 3wt% (Figure 3-B). Thus, salt in the digestate both inhibited and promoted nitrogenous compound formation. Salt concentration of 1–3wt% had an inhibiting effect on the $\%N_{oil}$ that might be associated with the increasing

divalent cation concentrations identified by Topete-Bentancourt et al.[78] as blocking agents in Maillard intermediate formation. Salt content of 3-5wt% promoted nitrogenous compound formation due to the increased feedstock alkalinity, given that salts in the digestate are primarily carbonated salts.

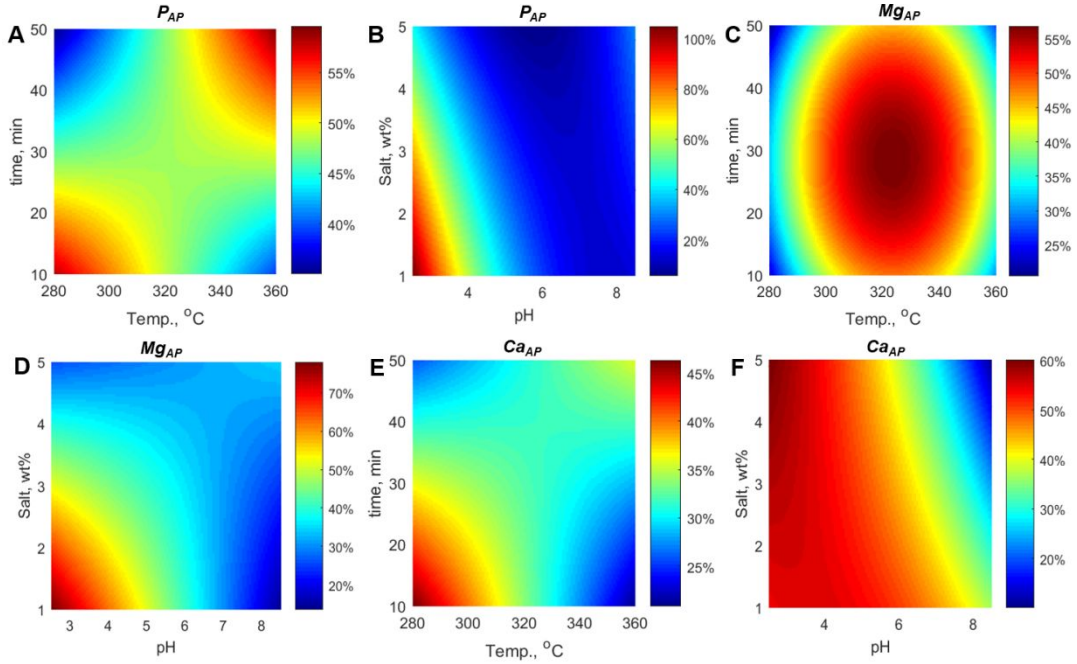

Figure 4. Representative contour plots of nutrient yield in HTL-AP: phosphorus (A, B), magnesium (C, D), and calcium (E, F).

The increasing feedstock alkalinity increased the feedstock pH and led to the formation of amides (***r*12** and ***r*31**) and N-heterocyclic compounds (***r*13** and ***r*14**) as indicated by compositional analysis of biocrudes from feedstock with salt content 5wt% in Table S7 (ESI).

3.3 Nutrient yield in HTL-AP

NH_3-N

The NH_3-N yield in HTL-AP (NH_3-N_{AP}) was between 18.21–52.03%, and was significantly correlated with reaction temperature and time, feedstock pH, and the Cel/Lig ratio on NH_3-N_{AP} (see Table 3). The reaction temperature and time showed a positive quadratic correlation with global minima at 330°C and 30 min, as illustrated in Figure 3-D. Figure 3-A and Figure 3-D show that the $\%N_{oil}$ and NH_3-N_{AP} were inversely correlated; the opposite shapes of the contour plots (valley-shaped versus mountain-shaped) indicates similar operating conditions (330°C and 30 min) for the global maxima and minima, respectively. This implies that a decrease in NH_3-N_{AP} was followed by an increase in $\%N_{oil}$, and vice versa, owing to nitrogen-fixing and nitrogen removal reactions that consumed and released NH_3, respectively. In addition, a negative interaction between reaction temperature and time (see Table 3) indicated that the highest NH_3-N_{AP} could be achieved by processing the digestates at 360°C for 10 min or 280°C for 50 min.

An expected inverse relationship between NH_3-N_{AP} and $\%N_{oil}$ was also observed at different feedstock pH values. However, the positive interaction between feedstock pH and reaction temperatures created a slightly different trend for NH_3-N_{AP} at the region of pH >6 and temperature >330°C. The observed decreasing trend for NH_3-N_{AP} at pH 2.5–6 and reaction temperatures ≤330°C (Figure 3-E) was replaced by a flat plateau indicating stabilized NH_3-N_{AP} at ~30-40%. The stabilized NH_3-N_{AP} may be associated with the hydro-denitrogenation of biocrudes at higher temperatures expelling a sufficient amount of nitrogen as NH_3-N to offset the amount of NH_3-N fixed into biocrudes. The mechanism of hydro-denitrogenation is discussed in subsection 3.2.2.

For different Cel/Lig ratios, no inverse relationship between NH_3-N_{AP} and $\%N_{oil}$ was observed: the Cel/Lig ratio showed a negative quadratic effect (instead of negative linear effect) on NH_3-N_{AP} with maxima at 0.75 (see Table 3 and Figure 3-F). The decrease in NH_3-N_{AP} with a Cel/Lig ratio decrease from 0.75 to 0.2 indicated that although nitrogen fixation into biocrude was inhibited at lower Cel/Lig ratios (sub-section 3.2.2), NH_3-N was still consumed by lignin decomposition products, generating aqueous-phase nitrogenous products. NH_3-N may react with lignin-derived phenols and carboxylic acids, thus producing amines (e.g., 4-aminophenol, 2,6-dimethylaniline, and benzidine) and amides (e.g., dimethylbenzamide, acetamide, and methacrylamide), respectively (see Table S8, ESI), via condensation reactions (***r*26** and ***r*12**).[79–81]

Phosphorus (P)

The phosphorus yield in HTL-AP (P_{AP}) obtained from HFCCD experiments was 4.94–77.02%. Feedstock pH was the most statistically significant factor with a quadratic relationship (see Table 3), exhibiting minima at pH ~6 (Figure 4-B). The quadratic relationship between P_{AP} and feedstock pH showed the same trend as the pH-dependent solubility isotherm of brushite ($CaHPO_4.2H_2O$) in the $Ca(OH)_2$-H_3PO_4-H_2O ternary system and $Ca(OH)_2$-H_3PO_4-HCl-H_2O quaternary system.[82] This similarity was expected because phosphorus in the digestate existed mostly as brushite, thus revealing two primary mechanisms accounting for the P_{AP} increase at more acidic and more alkaline feedstock pH.

First, phosphorus from more acidic feedstock was increasingly partitioned into HTL-AP because phosphate minerals are more soluble at lower pH (***r*48**). Secondly, the observed increase of P_{AP} at feedstock pH >6 was associated with H_3PO_4 release into the HTL-AP after brushite hydrolysis (***r*46** and ***r*47**) into the more thermodynamically stable hydroxyapatite ($Ca_{10}(PO_4)_6OH_2$) and whitlockite ($Ca_9MgHPO_4(PO_4)_6$).[83] The hydrolysis of brushite occurred at alkaline pH because hydroxyapatite and whitlockite were observed only in the hydro-char produced from alkaline feedstock (pH 8.5, see Figure S15 E, ESI), but they were not detected in the hydro-char produced from acidic feedstock (see Figure S15 D, ESI).

The second and the third most important factors for P_{AP} were salt content and the Cel/Lig ratio. The salt content was negatively correlated with P_{AP}. Higher salt content may increase the reaction medium alkalinity, as demonstrated by the positive linear effect of salt content on ΔpH_{liq} (see Table 3). Consequently, phosphate mineral solubility decreased, and P_{AP} decreased. In addition, a positive interaction was observed between salt content and feedstock pH (see Table 3); thus, P_{AP} slightly increased with increasing salt content in alkaline feedstock (Figure 4-B). However, increasing the Cel/Lig ratio in the feedstock yielded more phosphorus in HTL-AP because cellulose degradation through the acidic or alkaline pathway produced acids as side products, dissolving phosphate minerals. The acid production was confirmed by the negative linear effect of the Cel/Lig ratio on ΔpH_{liq} (see Table 3). However, a slight P_{AP} decrease was observed with increasing Cel/Lig ratio in the alkaline feedstock (see Figure S10, ESI), due to the negative interaction between Cel/Lig ratio and feedstock pH (see Table 3). A negative interaction was also observed between the Cel/Lig ratio and salt content, thus resulting in a lower increase in P_{AP} with the Cel/Lig ratio at higher salt content (see Figure S10, ESI).

The effects of reaction temperature and time were less significant than the other factors, as indicated by the smaller values of their respective linear coefficients and their interaction term coefficient in Table 3. Nevertheless, the observed positive interaction between those two factors revealed that higher P_{AP} could be achieved with HTL at more severe conditions (Figure 4-A), under which the ability to extract more phosphorus into HTL-AP was attributed to the enhanced acid production, as demonstrated by the coefficients of the linear and interaction terms of reaction temperature and time in the ΔpH_{liq} model (see Table 3).

Calcium (Ca) and Magnesium (Mg)

The yield of calcium and magnesium in HTL-AP (Ca_{AP} and Mg_{AP}) was 11.24–56.01% and 5.43–93.68%, respectively. Both Ca_{AP} and Mg_{AP} decreased significantly when the feedstock pH increased (see Table 3, Figure 4-D, and Figure 4-F), because the solubility of calcium and magnesium minerals negatively correlated with pH. Similarly, higher salt content produced lower Ca_{AP} and Mg_{AP} because the increased alkalinity in the digestate from the presence of more carbonate salts may retain calcium and magnesium in the solid phase as calcite (a trigonal-structured polymorph of $CaCO_3$, ***r*38**), lansfordite ($MgCO_3.5H_2O$, ***r*40**), and hydromagnesite ($Mg_5(CO_3)_4(OH)_2{\cdot}4H_2O$, ***r*43**), as shown in Figure S15 (ESI). However, the Mg_{AP} decrease at higher salt content was observed only at feedstock pH ≤6.5 due to the positive interaction between feedstock pH and salt content (see Table 3). At feedstock pH >6.5, Mg_{AP} was relatively constant at ~25% at any feedstock salt content (see Figure S12, ESI). Meanwhile, the observed negative interaction between feedstock pH and salt content in the Ca_{AP} model (see Table 3) resulted in a steeper decrease in Ca_{AP} at higher feedstock pH and salt contents.

The Cel/Lig ratio had a statistically significant effect on only Ca_{AP} (see Table 3). Higher Cel/Lig ratios linearly increased Ca_{AP} because higher cellulose content enabled the production of more acids, which decreased the pH and increased the solubility of calcium minerals. Nevertheless, because of the negative relationship between the salt content and Cel/Lig ratio, the Ca_{AP} increase gradually disappeared at higher feedstock salt content. A feedstock salt content of 4wt% was the inflection point of the slope of Ca_{AP}. Thus, higher Cel/Lig ratios in high-salinity feedstock (>4wt%) resulted in lower Ca_{AP} because carbonate salts may provide a high buffering capacity that resist the decrease in reaction medium pH.

The HTL operating conditions showed different effects on Ca_{AP} and Mg_{AP}. Increasing the reaction temperature at reaction times ≤35 min decreased Ca_{AP} (Figure 4-E), in accordance with the solubility of calcium minerals, such as $CaCO_3$, that negatively correlated with temperature. However, Ca_{AP} increased under higher temperatures and a reaction time >35 min. The mechanisms underlying these findings may be associated with the phase transition of less soluble to more soluble calcium minerals. The dominating polymorphs of $CaCO_3$ were aragonite and vaterite in the hydro-char produced from more-severe conditions (see Figure S15 C, ESI). In contrast, calcite was the only detected $CaCO_3$ polymorph in the hydro-char produced from less-severe conditions (see Figure S15 A, D, and E, ESI). Aragonite and vaterite are orthorhombic and hexagonal polymorphs of $CaCO_3$, respectively, which are more soluble than calcite (trigonal-structured). Because aragonite is the most stable phase of $CaCO_3$ at high pressure, more-severe conditions (including higher pressures) can induce the phase transformation of calcite into aragonite (***r*37**).[84] Meanwhile, the establishment and stabilization of vaterite under more severe conditions was promoted by increased production of hydrophilic organic macromolecules (***r*39**), e.g., phenols,

aldehydes, and ketones,[85] which may create hydrogen-bonded networks with water and deplete free H_2O molecules. Consequently, the initially formed vaterite crystals did not readily transform into calcite and continued to aggregate and precipitate, forming more vaterites.[86]

The reaction temperature and time had quadratic effects on Mg_{AP} (see Table 3), yielding global maxima at 320°C and 30 min, respectively (Figure 4-C). Mg_{AP} increased at 280–320°C because magnesium in hydro-char existed mostly as lansfordite ($MgCO_3.5H_2O$, see Figure S15 A, ESI), whose solubility increases with temperature.[87] At temperatures >320°C, nesquehonite ($MgCO_3.3H_2O$) was the primary magnesium mineral in the hydro-char (see Figure S15 B, ESI). This suggests that lansfordite was dehydrated into nesquehonite (***r*41**). Because the solubility of nesquehonite decreases with temperature,[87] at >320°C, Mg_{AP} decreased. At a reaction time >30 min, more-hydrated magnesium carbonates were dehydrated (***r*41** and ***r*42**); in addition, nesquehonite formation at 280–320°C (after previous production of mostly lansfordite at reaction times <30 min) and magnesite (anhydrous $MgCO_3$) formation at 320–360°C (after the previous production of mostly nesquehonite at reaction time <30 min) were enhanced (see Figure S15 A, B, and C, ESI). The formation of less-hydrated Mg-carbonates at a reaction time >30 min may explain the Mg_{AP} decrease at 30–50 min because less-hydrated phases were less soluble than the more-hydrated phases.[87]

4. Optimization and validation of HTL operating conditions

This section describes the multi-objective optimization and presents the optimal ranges of reaction temperature, reaction time, and feedstock pH leading to maximum energy and nutrient recoveries based on the different feedstock compositions. The validation of the optimization results is also presented.

The optimal conditions to achieve the optimization objectives were achieved over the range of Cel/Lig ratios and salt contents studied (see Figure 5). The composite desirability and the values of optimized responses at these optimal conditions are given in Figure S16-S17 (ESI). In general, an initial feedstock pH of ~3.00–3.90 is suitable for processing digestates containing salt <4wt% (Figure 5-C). Acidic conditions increased biocrude production and nutrient yield in HTL-AP and inhibited nitrogen fixation in biocrude and recondensation of oily lignin monomers into hydro-char. However, at a salt content ≥4wt%, a less acidic pH for the digestate (3.91–5.53) and HTL operation at 343–354°C are recommended (Figure 5-A).

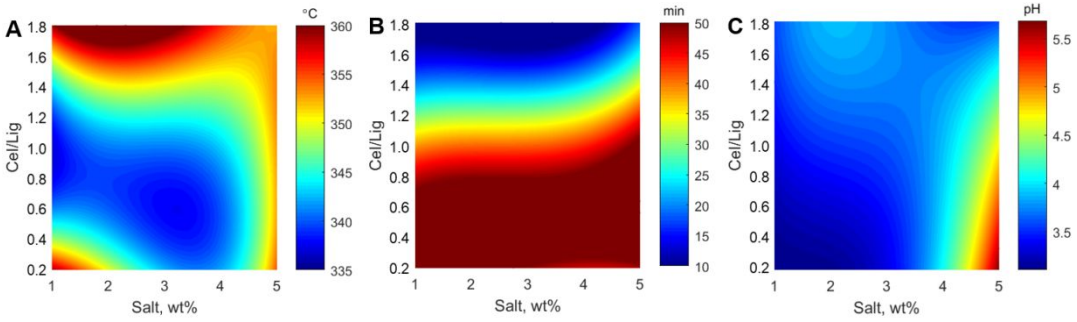

Figure 5. Contour plots of optimal (A) reaction temperature, (B) reaction time, and (C) feedstock pH for processing digestates with cellulose-to-lignin ratio (Cel/Lig) 0.2–1.8 and salt content 1–5wt%.

Table 4. Validation results for multi-objective optimization. Pred. = predicted value; Exp. = experimental value; and Diff. = difference between Pred. and the average value of Exp.

Optimized Responses	Digestate 1 Salt: 2 wt% Cel/Lig: 0.4 T: 348.7°C t: 50 min pH: 3.23			Digestate 2 Salt: 2 wt% Cel/Lig: 1.6 T: 359.2°C t: 10 min pH: 3.53			Digestate 3 Salt: 4 wt% Cel/Lig: 0.4 T: 339.6°C t: 50 min pH: 3.77			Digestate 4 Salt: 4 wt% Cel/Lig: 1.6 T: 354.3°C t: 10 min pH: 3.77		
	Pred. (%)	Exp. (%)	Diff. (%)	Pred. (%)	Exp. (%)	Diff. (%)	Pred. (%)	Exp. (%)	Diff. (%)	Pred. (%)	Exp. (%)	Diff. (%)
$Y_{oil,daf}$	42.7	42.6 ± 0.2	0.1	42.4	42.6 ± 0.4	-0.2	36.0	35.4 ± 0.6	0.6	34.9	35.2 ± 0.1	-0.3
ER_{oil}	63.4	63.2 ± 0.3	0.2	71.0	70.4 ± 0.6	0.6	61.7	61.8 ± 0.3	-0.1	66.0	65.5 ± 0.5	0.5
$\%O_{DWO}$	32.8	32.9 ± 0.3	-0.1	38.9	39.4 ± 0.6	-0.5	32.4	32.1 ± 0.4	0.3	37.0	37.0 ± 0.3	0.0
$\%O_{DSO}$	23.6	24.0 ± 0.5	-0.4	25.3	25.9 ± 0.3	-0.6	17.4	17.4 ± 0.5	0.0	22.2	22.5 ± 0.2	-0.3
$\%N_{DWO}$	0.4	0.4 ± 0.1	0.0	0.0	0.1 ± 0.0	0.0	1.2	1.1 ± 0.1	0.1	0.3	0.2 ± 0.3	0.1
$\%N_{DSO}$	0.1	0.1 ± 0.1	0.0	0.3	0.4 ± 0.1	-0.1	0.4	0.4 ± 0.1	0.0	0.5	0.6 ± 0.0	-0.1
P_{AP}	49.6	49.2 ± 0.3	0.4	74.8	74.2 ± 0.4	0.6	24.8	25.3 ± 0.6	-0.5	33.7	33.6 ± 0.3	0.1
NH_3-N_{AP}	46.5	46.4 ± 0.2	0.1	52.0	52.3 ± 0.6	-0.3	44.7	44.9 ± 0.4	-0.2	49.2	48.9 ± 0.4	0.3
Mg_{AP}	75.2	75.3 ± 0.5	-0.1	65.3	64.6 ± 0.7	0.7	68.1	67.6 ± 0.4	0.5	61.4	61.7 ± 0.4	-0.3

Ca_{AP}	36.3	36.1 ± 1.0	0.2	36.2	37.6 ± 0.1	-1.4	40.7	40.7 ± 0.9	0.0	30.3	29.9 ± 0.4	0.4

According to the desirability plots (see Figure S18, ESI), higher salt content decreased the individual desirability of biocrude yield, ER_{oil}, P_{AP}, and $\%N_{oil}$. Adjusting the digestate pH to ~3.91–5.53 may improve the individual desirability of biocrude yield and ER_{oil}, because a feedstock pH of ~4–5.5 provided the highest biocrude yield and energy recovery (see sub-section 3.1.1). Moreover, the improvements in P_{AP} and $\%N_{oil}$ were achieved by increasing the reaction temperature to 354°C to promote partial removal of nitrogen from biocrude as NH_3-N via HDN reactions (see sub-section 3.2.2) and to enhance phosphorus mineral dissolution into HTL-AP through acids production (see sub-section 3.3.2).

Similarly, higher reaction temperatures up to 360°C were required by cellulose-rich digestates (Cel/Lig >1, Figure 5-A) to expel nitrogen fixed by cellulose-derived carbonyl compounds into the biocrude (see sub-section 3.2.2 for denitrogenation mechanism). Combined with shorter reaction times, as suggested in Figure 5-B, the lowest $\%N_{oil}$ was 0.14–0.21% (see Figure S17, ESI). Meanwhile, a reaction time of 45–50 min and a reaction temperature of 337–358°C were required by lignin-rich digestates (Cel/Lig <1) to compensate for the adverse effects of higher lignin content (see Figure S18, ESI), i.e., lower ER_{oil}, lower P_{AP}, and higher $\%O_{oil}$.

The optimum HTL operating conditions were confirmed through five-time-replicated experimental validation test on digestates with four different compositions: 1). salt 2wt% and Cel/Lig 0.4; 2). salt 2wt% and Cel/Lig 1.6; 3). salt 4wt% and Cel/Lig 0.4; and 4). salt 4wt% and Cel/Lig 1.6. The small differences between the predicted and experimental values of all optimized responses (see Table 4) demonstrate the response models' validity and accuracy for all investigated combinations of independent variables.

5. Summary of experimentally validated reaction pathways for optimized conditions

In summary, at optimized HTL process condition (e.g., acidic feedstock pH), the biocrude oil is produced from cellulose and lignin conversion into cyclic (C_{5-} and C_6-) ketones (***r*7**), alkyl-furans (***r*8**), alkyl-methoxyphenols (***r*29**), C_2-aldehyde-susbtituted phenols (***r*21**), benzodioxanes (***r*25**), benzodioxolanes (***r*23**), and benzopyrans (***r*22**). However, cellulose is also converted into soluble compounds that partition in the AP, for example from acid-catalyzed retro-aldol condensation (***r*9**) of carbohydrate monomers (e.g., α-hydroxycarbonyls, α-dicarbonyls, acids, and aldehydes) and acid-catalyzed rehydration (***r*3**) of 5-HMF (i.e., levulinic acid and formic acid), while lignin acidolysis (***r*21**) produces aqueous-phase organics such as phenols, hydroxy-phenols, phenolic acids (***r*19**), and aromatic amines (***r*26**). In addition, acidic feedstock pH enhances nitrogen fixation in the biocrude through Paal-Knorr condensation reaction (***r*15**) between α-dicarbonyls and NH_3 or amino acid to form pyrroles, and through Beckmann rearrangement (***r*28**) of phenol-derived cyclic C_6-ketones into caprolactam. Processing the digestates at high reaction temperatures and long processing times remove nitrogen from biocrude as NH_3-N through hydro-denitrogenation, by converting N-heterocyclic compounds into aliphatic alkanes through aromatic-ring saturation (***r*16**) and opening (***r*17**) and alkylamine deamination (***r*18**). The low pH also partitions most of the Mg and P into AP by enhancing their solubilities (***r*48** and ***r*49**), while Ca mostly precipitates in the hydrochar as calcite (***r*38**), aragonite (***r*37**), and vaterite (***r*39**), due to its lower solubility compared to Mg and P minerals.

6. Conclusions and Recommendations

An experimental study of hydrothermal liquefaction (HTL) of selected model anaerobic digestates representative of dairy waste feedstocks was conducted. A comprehensive HTL reaction pathway for anaerobic digestate was proposed based on interpretations of the statistical analysis results of our experimental study and their comparison with the available published results from earlier studies. A range of waste compositions and experimental conditions: HTL temperature of 280–360°C, reaction time of 10–50 min, feedstock pH of 2.5–8.5, digestate salt content of 1–5wt%, and digestate cellulose-to-lignin ratio of 0.2–1.8. Thirty-two HTL experiments were conducted following a response surface design methodology based on a half-fractional central composite design. The HTL products of each run are analyzed using elemental analysis, GC-MS, XRD, and colorimetric techniques. Using the results from these analyses, quadratic regression equations for each response variables are obtained. Subsequently in analyzing the data, a desirability function approach was used to specify the HTL conditions that simultaneously maximize biocrude energy recovery, minimize biocrude heteroatom content, maximize nutrient yield (i.e., NH_3-N, Mg, and P) in the aqueous-phase coproduct for the different digestate compositions. Additional HTL experiments validated this optimization method and its accuracy.

The optimization results uncover the mechanistic significance of pre-acidifying the feedstock (pH 3.00–5.53) using acetic acid and processing at high reaction temperatures (337–360°C) and at a broad range of reaction times (10–50 min) depending on the cellulose-to-lignin ratio for maximum biocrude energy recovery and nutrient yield in HTL-AP. At such conditions, the biocrude yield is maximized as cellulose is converted into pyrones, cyclic ketones, furanones, and aliphatic alkanes while lignin into alkyl-substituted methoxyphenols, hydroxymethylated phenols, dioxanes/dioxolanes, and pyrans. Moreover, the Maillard reaction (responsible for the formation of N-containing formation α-dicarbonyls and α-hydroxycarbonyls in the oil) is inhibited, and deoxygenation and hydro-denitrogenation contribute to minimizing the biocrude heteroatom content. Nutrients (i.e., NH_3-N, P, and Mg) are effectively partitioned in the aqueous phase as acidic conditions

prevent them from precipitating as hydroxyapatite, whitlockite, or $MgCO_3$ minerals in the hydrochar. The only exception is Ca, which effectively precipitates as calcite in the solid hydrochar phase.

The nutrients partitioned into the aqueous phase product (HTL-AP) will need to be recovered ultimately to demonstrate economic viability with a more sustainable outcome, consistent with achieving a circular bioeconomy. A possible pathway for recovery of both N and P is to crystallize struvite from the HTL aqueous phase. Future studies are required to describe and optimize the struvite crystallization process from actual wastewater. This topic will be the target of a future publication. In addition, while this work demonstrates the possibility of simultaneously optimizing both energy recovery in biocrude and nutrient yield in the aqueous phase coproduct, the determined optimal HTL operating conditions require high temperatures and large quantities of acetic acid to control the feedstock pH, which may not be economically viable. Future research should therefore identify alternatives to acetic acid (i.e., other inexpensive organic acids, or heterogeneous solid acid catalysts) that can maximize energy and nutrient recovery for digestate using HTL at milder operating conditions to lower the operational cost of HTL.

Conflicts of interest

The authors declare no conflicts of interest to disclose.

Author Contributions

Hanifrahmawan Sudibyo: conceptualization, methodology, formal analysis, investigation, data curation, visualization, and writing – original draft. **Matteo Pecchi**: conceptualization, formal analysis, visualization, and writing – review & editing. **Jefferson William Tester**: conceptualization, methodology, writing – review & editing, supervision, and funding acquisition.

Acknowledgements

This study was funded in part by the Cornell Energy Systems Institute, the Graduate School at Cornell, the U.S. Department of Energy (DOE) through their RAPID program, and the USDA grant 2019-69012-29905 that involves collaborative research between Cornell University and the University of Arkansas. This study also utilized the Cornell Center for Materials Research Shared Facilities (NSF MRSEC DMR-1719875). The authors thank Dr. Kui Wang for providing technical assistance during the experimental work performed as part of this study. The first author also thanks to the Fulbright-DIKTI Foundation for support as a doctoral candidate in chemical engineering at Cornell University.

References

1 NCBA, Beef Industry Overview, https://www.ncba.org/producers/industry-statistics, (accessed May 16, 2021).
2 United States Environmental Protection Agency, *2018 Wasted Food Report*, Washington D.C., 2020.
3 H. Sudibyo, Z. L. Shabrina, L. Halim and W. Budhijanto, *Energy Procedia*, 2017, **105**, 256–262.
4 R. Nkoa, *Agronomy for Sustainable Development*, 2014, **34**, 473–492.
5 Zeshan and C. Visvanathan, *International Biodeterioration and Biodegradation*, 2014, **95**, 167–175.
6 G. A. Iocoli, M. C. Zabaloy, G. Pasdevicelli and M. A. Gómez, *Science of the Total Environment*, 2019, **647**, 11–19.
7 C. Le Maréchal, C. Druilhe, E. Repérant, E. Boscher, S. Rouxel, S. Le Roux, T. Poëzévara, C. Ziebal, C. Houdayer, B. Nagard, F. Barbut, A. M. Pourcher and M. Denis, *MicrobiologyOpen*, 2019, **8**, 1–10.
8 W. Wang and D. J. Lee, *Bioresource Technology*, 2021, **323**, 124626.
9 A. A. Peterson, F. Vogel, R. P. Lachance, M. Fröling, M. J. Antal and J. W. Tester, *Energy and Environmental Science*, 2008, **1**, 32–65.
10 M. Pecchi and M. Baratieri, *Renewable and Sustainable Energy Reviews*, 2019, **105**, 462–475.
11 Y. Fan, U. Hornung, N. Dahmen and A. Kruse, *Biomass Conversion and Biorefinery*, 2018, **8**, 909–923.
12 R. Posmanik, D. A. Cantero, A. Malkani, D. L. Sills and J. W. Tester, *Journal of Supercritical Fluids*, 2017, **119**, 26–35.
13 R. Obeid, D. M. Lewis, N. Smith, T. Hall and P. van Eyk, *Chemical Engineering Journal*, 2020, **389**, 1–14.
14 J. Yang, Q. (Sophia) He, K. Corscadden, H. Niu, J. Lin and T. Astatkie, *Applied Energy*, 2019, **233–234**, 906–915.
15 T. Yang, Y. Jie, B. Li, X. Kai, Z. Yan and R. Li, *Fuel Processing Technology*, 2016, **148**, 19–27.
16 F. Cheng, G. A. Tompsett, D. V. Fraga Alvarez, C. I. Romo, A. M. McKenna, S. F. Niles, R. K. Nelson, C. M. Reddy, S. Granados-Fócil, A. D. Paulsen, R. Zhang and M. T. Timko, *Sustainable Energy and Fuels*, 2021, **5**, 941–955.
17 R. Posmanik, C. M. Martinez, B. Cantero-Tubilla, D. A. Cantero, D. L. Sills, M. J. Cocero and J. W. Tester, *ACS Sustainable Chemistry and Engineering*, 2018, **6**, 2724–2732.
18 X. Zhang, K. Wilson and A. F. Lee, *Chemical Reviews*, 2016, **116**, 12328–12368.
19 B. M. Ghanim, W. Kwapinski and J. J. Leahy, *ACS Sustainable Chemistry and Engineering*, 2018, **6**, 11265–11272.
20 H. Sudibyo, K. Wang and J. W. Tester, *ACS Sustainable Chemistry and Engineering*, 2021, **9**, 11403–11415.
21 Q. Wang, H. Jung, B. Wan, P. Liu, P. Yang and Y. Tang, *ACS Sustainable Chemistry and Engineering*, 2021, **9**, 10630–10641.
22 D. Crutchik and J. M. Garrido, *Chemosphere*, 2016, **154**, 567–572.
23 U. Ekpo, A. B. Ross, M. A. Camargo-Valero and P. T. Williams, *Bioresource Technology*, 2016, **200**, 951–960.

24 U. Ekpo, A. B. Ross, M. A. Camargo-Valero and L. A. Fletcher, *Bioresource Technology*, 2016, **214**, 637–644.
25 N. R. Costa, J. Lourenço and Z. L. Pereira, *Chemometrics and Intelligent Laboratory Systems*, 2011, **107**, 234–244.
26 K. Möller and T. Müller, *Engineering in Life Sciences*, 2012, **12**, 242–257.
27 Y. Zhong, Z. Liu, C. Isaguirre, Y. Liu and W. Liao, *Biotechnology for Biofuels*, 2016, **9**, 1–11.
28 K. Risberg, H. Cederlund, M. Pell, V. Arthurson and A. Schnürer, *Waste Management*, 2017, **61**, 529–538.
29 K. Güngör and K. G. Karthikeyan, *Bioresource Technology*, 2008, **99**, 425–436.
30 W. Tao, K. P. Fattah and M. P. Huchzermeier, *Journal of Environmental Management*, 2016, **169**, 46–57.
31 American Society for Testing and Materials (ASTM), *ASTM E1131-20 Standard Test Method for Compositional Analysis by Thermogravimetry*, West Conshohocken, Pennsylvania, 2015, vol. 08.
32 S. A. Channiwala and P. P. Parikh, *Fuel*, 2002, **81**, 1051–1063.
33 American Society for Testing and Materials (ASTM), *ASTM D1426-15 Standard Test Methods for Ammonia Nitrogen In Water*, United States, 2015.
34 APHA (American Public Health Association), *Standard Methods for the Examination of Water and Wastewater*, APHA (American Public Health Association), Washington D.C., 20th edn., 1999.
35 K. S. Crane, B. L. Webb, P. S. Allen and V. D. Jolley, *Communications in Soil Science and Plant Analysis*, 2005, **36**, 2687–2697.
36 Environmental Protection Agency (EPA), in *Test Methods for Evaluating Solid Waste, Physical/Chemical Methods SW-846*, Environmental Protection Agency (EPA), Washington D.C., 3rd edn., 2015, pp. 1–5.
37 M. F. Ryan and H. Barbour, *Annals of Clinical Biochemistry*, 1998, **35**, 449–459.
38 R. W. Wells, *American Journal of Clinical Pathology*, 1948, **18**, 576–578.
39 R. B. Madsen, M. M. Jensen, A. J. Mørup, K. Houlberg, P. S. Christensen, M. Klemmer, J. Becker, B. B. Iversen and M. Glasius, *Analytical and Bioanalytical Chemistry*, 2016, **408**, 2171–2183.
40 D. C. Montgomery and G. C. Runger, in *Applied Statistics and Probability for Engineers*, John Wiley and Sons, Inc., New York, NY, 3rd edn., 2002, p. subsection 14-10.
41 C. Yang, S. Wang, J. Yang, D. Xu, Y. Li, J. Li and Y. Zhang, *Green Chemistry*, 2020, **22**, 8210–8232.
42 W. Schutyser, T. Renders, S. Van Den Bosch, S. F. Koelewijn, G. T. Beckham and B. F. Sels, *Chemical Society Reviews*, 2018, **47**, 852–908.
43 J. Yang, Q. (Sophia) He, K. Corscadden, H. Niu, J. Lin and T. Astatkie, *Applied Energy*, 2019, **233–234**, 906–915.
44 M. H. Marzbali, S. Kundu, P. Halder, S. Patel, I. G. Hakeem, J. Paz-Ferreiro, S. Madapusi, A. Surapaneni and K. Shah, *Chemosphere*, 2021, **279**, 130557.
45 T. Shen, R. Hu, C. Zhu, M. Li, W. Zhuang, C. Tang and H. Ying, *RSC Advances*, 2018, **8**, 37993–38001.
46 S. Al-Hammadi and G. da Silva, *Physical Chemistry Chemical Physics*, 2021, **23**, 2046–2054.
47 M. Chatterjee, T. Ishizaka and H. Kawanami, *Green Chemistry*, 2018, **20**, 2345–2355.
48 J. N. M. Tan-Soetedjo, H. H. Van De Bovenkamp, R. M. Abdilla, C. B. Rasrendra, J. Van Ginkel and H. J. Heeres, *Industrial and Engineering Chemistry Research*, 2017, **56**, 13228–13239.
49 F. Jin and H. Enomoto, *Energy and Environmental Science*, 2011, **4**, 382–397.
50 M. R. Sturgeon, S. Kim, K. Lawrence, R. S. Paton, S. C. Chmely, M. Nimlos, T. D. Foust and G. T. Beckham, *ACS Sustainable Chemistry and Engineering*, 2014, **2**, 472–485.
51 S. Huang, N. Mahmood, M. Tymchyshyn, Z. Yuan and C. C. Xu, *Bioresource Technology*, 2014, **171**, 95–102.
52 S. Liu, J. Han, Q. Wu, B. Bian, L. Li, S. Yu, J. Song, C. Zhang and A. J. Ragauskas, *Catalysis Letters*, 2019, **149**, 2383–2389.
53 L. Shuai and B. Saha, *Green Chemistry*, 2017, **19**, 3752–3758.
54 L. Shuai, M. T. Amiri, Y. M. Questell-Santiago, F. Héroguel, Y. Li, H. Kim, R. Meilan, C. Chapple, J. Ralph and J. S. Luterbacher, *Science*, 2016, **354**, 329–333.
55 Z. Srokol, A. G. Bouche, A. Van Estrik, R. C. J. Strik, T. Maschmeyer and J. A. Peters, *Carbohydrate Research*, 2004, **339**, 1717–1726.
56 Z. Wang, in *Comprehensive Organic Name Reactions and Reagents*, John WIley & Sons, Inc., 2010, pp. 982–985.
57 W. Wang, Y. Liu, Z. Liu and S. Tian, *Energy and Fuels*, 2016, **30**, 968–974.
58 M. N. Islam, G. Taki, M. Rana and J. H. Park, *Industrial and Engineering Chemistry Research*, 2018, **57**, 4779–4784.
59 H. Pińkowska, P. Wolak and A. Złocińska, *Chemical Engineering Journal*, 2012, **187**, 410–414.
60 F. S. Chakar and A. J. Ragauskas, *Industrial Crops and Products*, 2004, **20**, 131–141.
61 C. Lapierre, in *Lignin and Lignans: Advances in Chemistry*, eds. C. Heitner, D. Dimmel and J. Schmidt, Boca Raton, 1st edn., 2010, pp. 11–48.
62 S. Kang, X. Li, J. Fan and J. Chang, *Renewable and Sustainable Energy Reviews*, 2013, **27**, 546–558.
63 E. Nagel and C. Zhang, *Industrial and Engineering Chemistry Research*, 2019, **58**, 18866–18880.
64 M. Li, Y. Pu and A. J. Ragauskas, *Frontiers in Chemistry*, 2016, **4**, 1–8.
65 Environmental Protection Agency (EPA), *Consolidated List of Reformulated Gasoline and Anti-Dumping Questions and Answers*, Washington D.C., 2003.
66 G. H. C. Prado, Y. Rao and A. De Klerk, *Energy and Fuels*, 2017, **31**, 14–36.
67 A. A. Peterson, R. P. Lachance and J. W. Tester, *Industrial and Engineering Chemistry Research*, 2010, **49**, 2107–2117.
68 Q. Zhang, J. M. Ames, R. D. Smith, J. W. Baynes and T. O. Metz, *Journal of Proteome Research*, 2009, **8**, 754–769.

69 V. A. Yaylayan, *Food Science and Technology Research*, 2003, **9**, 1–6.
70 X. Wu, M. Huang, F. Kong and S. Yu, *Journal of Dairy Science*, 2015, **98**, 8565–8571.
71 A. N. Yu, Z. W. Tan and F. S. Wang, *LWT - Food Science and Technology*, 2013, **50**, 64–71.
72 Y. S. Bao, B. Zhaorigetu, B. Agula, M. Baiyin and M. Jia, *Journal of Organic Chemistry*, 2014, **79**, 803–808.
73 R. Mocci, E. Colacino, L. De Luca, C. Fattuoni, A. Porcheddu and F. Delogu, *ACS Sustainable Chemistry and Engineering*, 2021, **9**, 2100–2114.
74 L. Zhang, J. Zhang, J. Ma, D. J. Cheng and B. Tan, *Journal of the American Chemical Society*, 2017, **139**, 1714–1717.
75 C. S. Raghuveer, J. W. Thybaut, R. De Bruycker, K. Metaxas, T. Bera and G. B. Marin, *Fuel*, 2014, **125**, 206–218.
76 Y. Guo, X. Liu, P. Duan, D. Xu and R. Luque, *ACS Sustainable Chemistry and Engineering*, 2021, **9**, 362–374.
77 B. de Falco, A. Petridis, P. Paramasivan, A. D. Troise, A. Scaloni, Y. Deeni, W. E. Stephens and A. Fiore, *RSC Advances*, 2020, **10**, 21535–21544.
78 A. Topete-Betancourt, J. de D. Figueroa Cárdenas, A. L. Rodríguez-Lino, E. Ríos-Leal, E. Morales-Sánchez and H. E. Martínez-Flores, *Food Science and Biotechnology*, 2019, **28**, 975–982.
79 S. Bugosen, I. D. Mantilla and F. Tarazona-Vasquez, *Heliyon*, 2020, **6**, e05778.
80 V. V. Bochkarev, L. S. Soroka, T. A. Klimova and L. E. Velikorechina, *Procedia Chemistry*, 2015, **15**, 320–325.
81 J. G. Speight, in *Handbook of Industrial Hydrocarbon Processes*, Gulf Professional Publishing, 2011, pp. 1–41.
82 L. C. Chow, *Monographs in Oral Science*, 2001, **18**, 94–111.
83 E. Boanini, F. Silingardi, M. Gazzano and A. Bigi, *Crystal Growth and Design*, 2021, **21**, 1689–1697.
84 P. N. Gavryushkin, N. Sagatov, A. B. Belonoshko, M. V. Banaev and K. D. Litasov, *Journal of Physical Chemistry C*, 2020, **124**, 26467–26473.
85 L. H. Fu, Y. Y. Dong, M. G. Ma, W. Yue, S. L. Sun and R. C. Sun, *Ultrasonics Sonochemistry*, 2013, **20**, 1188–1193.
86 L. Pérez-Villarejo, F. Takabait, L. Mahtout, B. Carrasco-Hurtado, D. Eliche-Quesada and P. J. Sánchez-Soto, *Ceramics International*, 2018, **44**, 5291–5296.
87 J. Li and X. Li, *Energies*, 2019, **12**, 1–16.